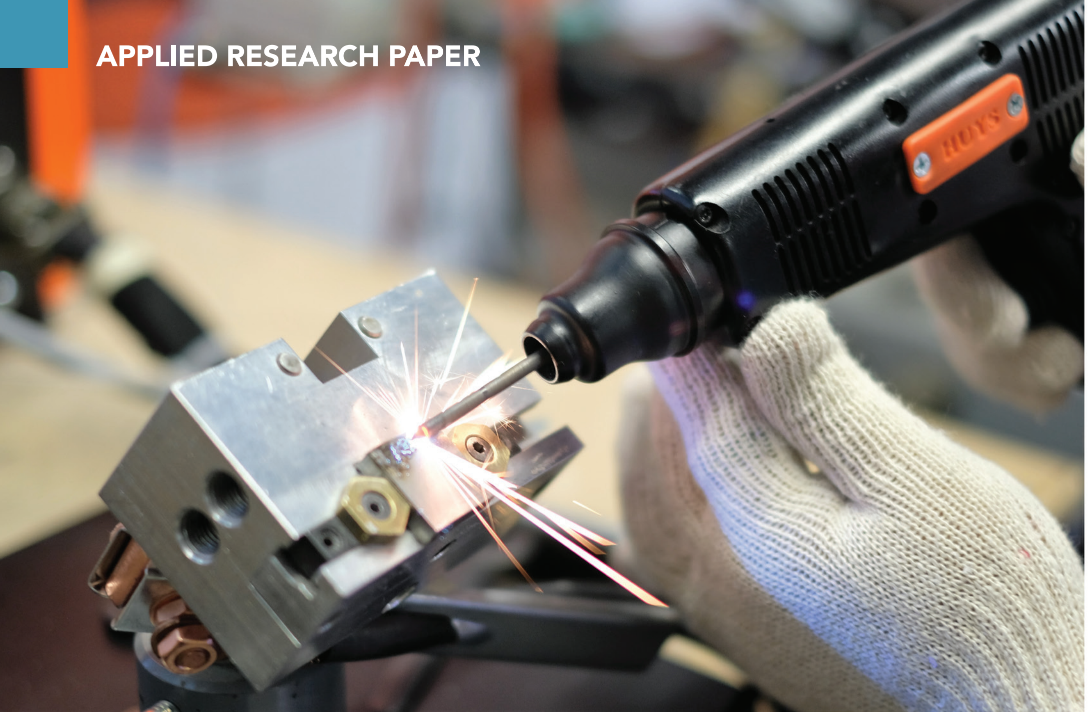

DEVELOPMENT OF **ELECTRO SPARK DEPOSITION TECHNOLOGY** FOR NI-SUPERALLOY REPAIR

1.0 INTRODUCTION

Electrospark deposition (ESD) has historically been used for the repair of small defects and the application of coatings on metal parts. It functions by repeatedly discharging a capacitor power supply through a consumable electrode, which transfers material to the substrate. This transfer occurs in the form of small molten droplets originating at the electrode, which splash onto the substrate surface and rapidly solidify. The atypical material transfer mechanism and capacitor-based power supply results in several advantages over other deposition processes. The required charging and discharging of the capacitor necessitates a cooling period after each transfer event, which allows heat to rapidly dissipate from the surface of the substrate. Additionally, the transfer of a small quantity of molten material with each capacitor discharge limits the amount of heat input. Because of the very rapid cooling rate, the part being coated or repaired remains at near ambient temperatures. This limits the size of the heat-affected zone (HAZ) and allows for the coating of materials that typically suffer from HAZ cracking, while also resulting in a fine-grained deposition that forms a metallurgical bond with the substrate. Consequently, coatings and repairs performed by ESD are denser and more strongly adhered to the substrate than those produced via cold spray, while resulting in less damage to the substrate when compared to laser cladding or directed energy deposition repair techniques.

An ESD process can be manually operated (Figure 1a), which makes use of a hand-held applicator to move the electrode across the substrate surface. An automated ESD system (Figure 1b) uses computer numerical controlled (CNC) or robotic systems to move the coating head and a force feedback control system to adjust the electrode contact with the substrate surface. The use case for manual and automated ESD systems are different, with manual systems more cost-effective when coating or repairing small areas or non-standard geometries. One example (shown in Figure 2) is the repair of damaged or eroded areas on turbine and compressor blades, with repairs performed on edge or surface defects once they are detected. However, an automated system is more effectively scaled for the deposition of large-area coatings or the coating/repair of multiple parts with the same geometry.

Fig. 1: Equipment provided by Huys Industries for a) manual and b) automated ESD coating and repair of components.

In addition to the repair of turbine engine components, ESD has broader applications in aerospace and other industries where components are exposed to harsh conditions. The ability to dimensionally restore worn or damaged components makes ESD useful in the automotive/transportation industry, where turbocharger turbine wheels, diesel engine injector nozzles, high-performance exhaust valves/manifolds and ship propellers can either be coated to extend their lifespan or repaired instead of being replaced. The energy, manufacturing and chemical processing industries also benefit from the coating and repair of components exposed to corrosive environments, including valves, moulds and dies. Several examples of the application of ESD have been reported, demonstrating the repair of components such as valves in nuclear power plants [1], generator rotor shafts [2], steering and diving control rods on submarines [3], helical gear shafts [4], and bearing housings [3], as well as the coating of components such as the interior surface of gun barrels [3] and seal ring surfaces [5].

The large number of electrical and physical parameters in an ESD process makes optimization a challenge. Electrical parameters such as power input, voltage, capacitance and spark frequency can be regulated by the operator in both manual and automated ESD systems. Some physical process parameters are controllable in manual systems, such as the gas type, gas flow rate and electrode rotation/vibration speed. However, the use of automated ESD systems allows for further control over other physical parameters which would otherwise be subject to operator discretion, such as electrode contact pressure and travel speed. While the ability to control a greater number of parameters is useful for reliability and repeatability of the ESD process, it greatly complicates process optimization. Fortunately, literature has identified a subset of parameters that have the greatest effect on deposition quality and deposition rate; capacitance and voltage are the two primary parameters optimized when the deposition of a new material is required. Analyzing the effect of these parameters on metallurgical features allows for the selection of optimized parameters.

When developing an ESD process for the repair of critical components made of high-cost materials – such as gas turbines and jet engines made of Ni-superalloys – special attention must be given to

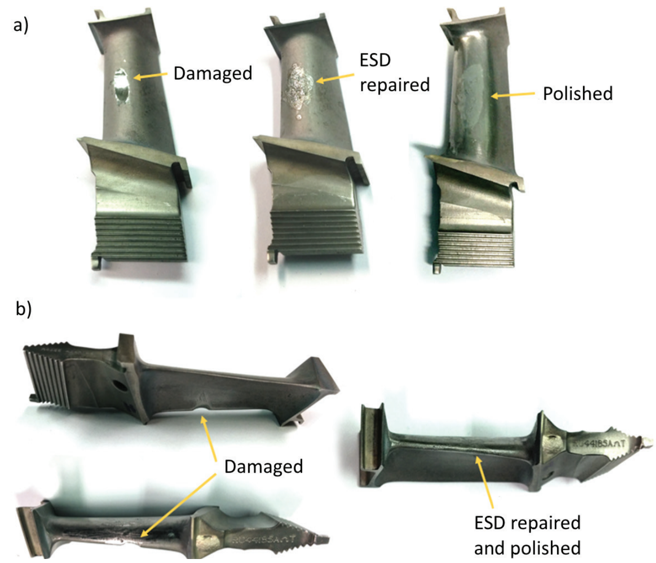

Fig. 2: Example of an ESD repaired turbine blade with a) surface damage and b) edge damage.

the microstructure of the deposited material. The ESD process parameters are closely linked to microstructural features that affect performance, which forms the basis of the commonly studied process-structure-property relationship. The following sections summarize the findings of several studies and introduce new data to evaluate the use of ESD technology for the repair of Inconel 718 Ni-superalloy parts.

2.0 EXPERIMENTAL

Sample characterization is performed on an Oxford BX51M optical microscope and a Zeiss UltraPlus scanning electron microscope (SEM) with an energy-dispersive X-ray spectroscopy (EDX) attachment. Sample preparation was performed according to the tests required, with further details provided in the following sections.

2.1 Parameter optimization

In order to determine an appropriate set of parameters for the repair of an Inconel 718 substrate, a manual ESD machine developed by Huys Industries was used to deposit Inconel 718 with all combinations from a chosen set of capacitance (80, 100 and 120 μF) and voltage (50, 100 and 120 V) parameters. The frequency was kept fixed at 170 Hz, as was the electrode diameter (3mm) and 5.0 grade argon shielding gas flow rate (10L/min). A total of 10 passes with the electrode in a 1 cm^2 region using a raster scan pattern

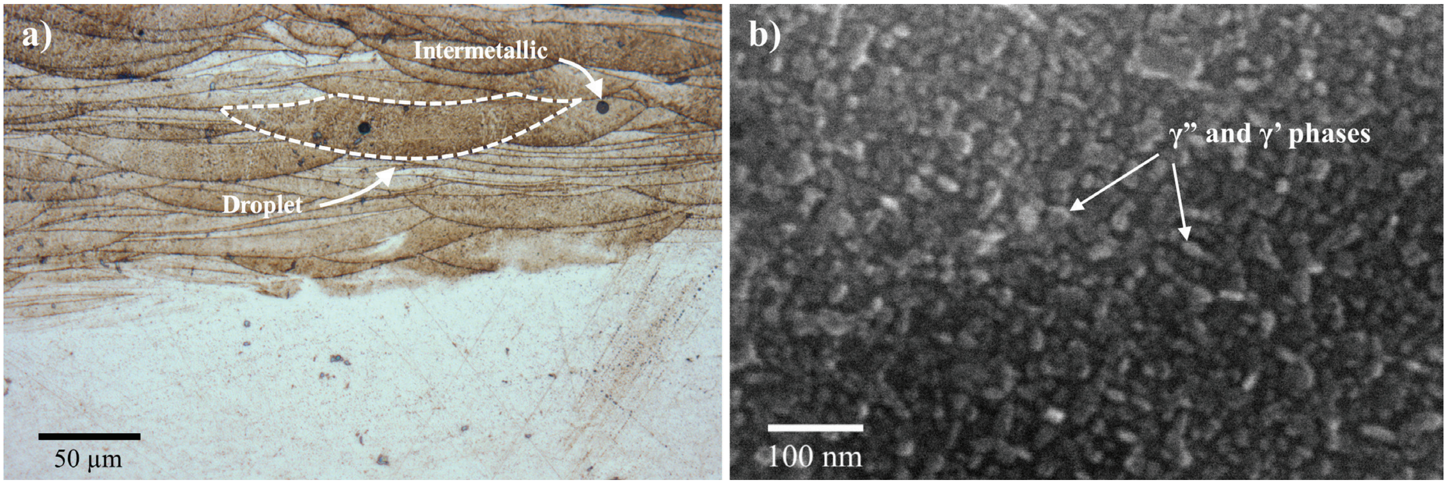

Fig. 3: Etched cross-section of Inconel 718 deposited on Inconel 718 substrate showing a) optical image of the droplet morphology and an intermetallic defect, and b) SEM image of γ″ and γ′ phases after an aging heat treatment

were used to apply the coating, and a hand-held peening tool was used after each pass. The composition of the Inconel 718 electrode and substrate are listed in Table 1.

TABLE 1. MEASUREMENTS OBTAINED VIA EDX OF INCONEL 718 COMPOSITION (WT%) [1]

	Ni	Cr	Nb	Mo	Ti	Al	Si	Fe
Base Metal	54.0	19.7	3.3	2.6	1.1	0.3	_	19.0
Electrode	53.7	19.2	3.8	2.8	1.0	0.3	0.2	19.0

2.2 Oxidation resistance testing

Inconel 718 specimens were cut in 6mm by 3mm by 1.5mm dimensions using a Struers Accutom-50 precision saw. Oxidation resistance testing was performed using thermogravimetric analysis (TGA). The ESD coatings were performed using the same conditions as the parameter optimization study, with voltage and capacitance fixed at 100 V and 80 µF, respectively. All sides were coated with 7 passes performed in a raster scan pattern, after which all specimens were then aged using a two-step process. Specimens were loaded in a horizontal tube furnace at room temperature and argon gas was used to purge the tube for 15 min. The temperature was ramped to 720 °C at 5 °C/min and held for 8 hours, after which it was furnace cooled to 620°C and held for 10 hours. At the conclusion of the holding period, the samples were removed from the furnace and water quenched.

Samples after aging demonstrated discoloration on their surface, likely due to the formation of an oxide layer when being removed from the furnace. Grinding with up to 600 grit SiC paper was used to remove the discoloration on coated and uncoated samples, while also serving to remove surface roughness introduced by the ESD process. Sample dimensions were individually measured with the use of a caliper to determine the true exposed surface area, which may vary due to imprecision during their fabrication, slight differences in coating thickness, and differences in the amount of material removed during grinding. During TGA testing, the initial temperature ramp was performed under argon atmosphere to prevent uncontrolled oxidation at lower temperatures, after which the inlet gas was switched to a 20% oxygen/80% nitrogen mixture at 10 mL/min to allow for oxidation.

3.0 RESULTS AND DISCUSSION

3.1 Microstructure of ESD processed Inconel 718

The droplet transfer mechanism occurring during ESD results in a unique microstructure that can be viewed in Figure 3a. After etching, the boundaries of the transferred droplets are visible, and their shape indicates that some re-melting of previously transferred material occurs when additional droplets are deposited. A wide variation in the thickness is also observed, although droplet thickness is typically larger when using higher pulse energy (higher voltage and capacitance). Variations in microhardness were identified between the droplets of different thickness, attributed to higher cooling rates in thinner droplets [7]. Lower capacitance and voltage parameters can therefore be expected to produce coatings or repairs with higher hardness. A similar trend was observed for the tensile strength of repaired specimens [8], however the hardness and strength is still not comparable to that of the precipitation hardened Inconel 718 used in components. Similar to the welding of Inconel 718 using other techniques, post-processing heat treatments are required to achieve a maximum hardness and strength [9].

Many of the most commonly used Ni superalloys are precipitation strengthened. Inconel 718 forms a roughly 20 nm sized Ni_3Nb strengthening phase known as γ'' when exposed to an aging heat treatment (720 °C for 8 h, 2 h ramp down to 620 °C, hold at 620 °C for 8 hours), as well as a less influential $Ni_3(Al,Ti)$ phase known as γ'. Both phases are difficult to image due to their small size and are also difficult to distinguish between each other (Figure 3b). In the as-deposited condition, ESD processed Inconel 718 does not have γ'' or γ' and therefore exhibits strengths similar to solution annealed (not strengthened) Inconel 718. Although the deposited Inconel 718 has much higher hardness than solution annealed Inconel 718, the presence of interdendritic phases and droplet boundaries contribute to a lower fracture toughness [8].

Exposure of ESD processed Inconel 718 to an aging heat treatment precipitates the γ'' and γ' phases, resulting in a slightly higher hardness (8%) and slightly lower ultimate strength (-8%) than the precipitation hardened base metal [6]. The lower ultimate strength is once again attributed to the presence of interdendritic phases and droplet boundaries. If an equivalent or higher strength than the base metal is required, a solution heat treatment (1100 °C for 1.5 h) is required prior to aging. However, the use of a solution heat treatment comes at the expense of grain growth in the base metal, which reduces the overall strength of the part being repaired. For this reason, a direct-aging heat treatment (where the solutionizing step is avoided) is recommended in some cases.

In addition to improving the strength of the deposited Inconel 718, the use of an aging heat treatment also strengthens the softened HAZ that forms when repairing precipitation hardened Inconel 718. A heat affected zone of 40 μm has been reported, with softening attributed to solutionizing of the γ'' and γ' phases [6]. Although this HAZ size is significantly smaller than other welding processes due to the smaller heat input of the ESD process, the use of a direct-aging heat treatment re-precipitates these phases and regains the base metal's strength.

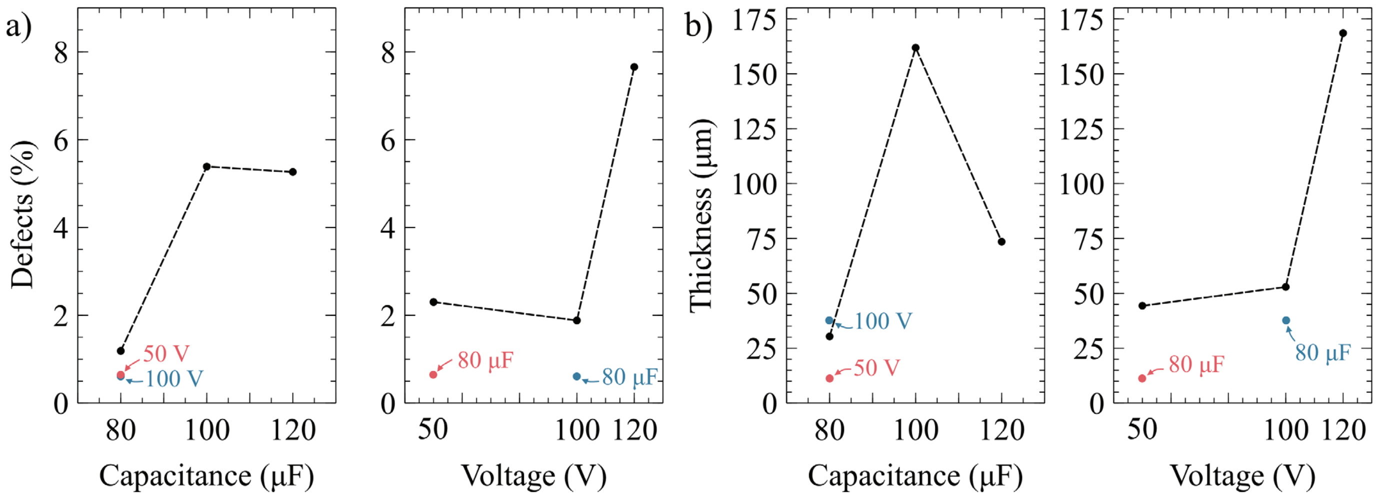

Fig. 4: Mean of means plots for capacitance and voltage factors with a) defects as a response variable and b) thickness of the deposited coatings as a response variable.

3.2 Process parameter optimization

Two measures are often used to evaluate the ESD process: the quantity of defects and deposition rate. Defects such as intermetallics or porosity are often detrimental to mechanical properties, acting as crack initiation sites and reducing the effective strength, whereas the deposition rate is important for industrial applications that depend on high throughput or shorter turnaround times. Unfortunately, the quantity of defects and deposition rate are often inversely related, with higher deposition rates resulting in more defects within the deposited material. The higher porosity is partially attributed to higher surface roughness with higher pulse energy, which encourages lack of fusion defects between subsequent depositions [10]. Additionally, the formation of detrimental intermetallics is reduced with lower energy input, as a result of more limited diffusion.

The use of an intermittent hand-held peening tool to mechanically deform the surface has proven effective at reducing the surface roughness between deposited layers. This results in a reduced quantity of defects, since lack of fusion porosities are less likely to form. For the repair of deeper cavities or thicker coatings, peening is necessary to prevent an excessive uneven buildup of deposited material. The careful selection of parameters can also be used to eliminate the need for post-process grinding or polishing, depending on the required surface roughness [10]. A surface roughness (arithmetic mean height) as low as 5 µm has been obtained when using optimized ESD parameters in conjunction with intermittent peening. Applications that require further reduction in surface roughness would require further processing.

The overall trends can be observed in the mean of mean plots in Figure 4, which show increasing defects with higher capacitance and voltage, whereas the deposition thickness for a fixed deposition time generally increases with higher capacitance and voltage. Two sets of process parameters that exhibit the fewest defects are highlighted in Figure 4 and although the deposition thickness is noticeably different between the two, they both remain low when compared to other studied parameters. To overcome the lower deposition rates, longer deposition times are required when depositing thicker coatings or repairing components.

Although the optimized parameters produce good quality depositions when applying Inconel 718 as a coating or performing most repairs, increased substrate temperatures and erosion due to poor heat transfer were issues when repairing thin regions of less than 200 µm. The ability to accurately control travel speed and electrode contact force in automated systems improves the deposition of material in these situations.

The test specimen in Figure 5a shows the manual buildup of a thin ridge approximately one millimeter in height, which suffers from significant lack of fusion porosities (Figure 5b). However, the use of an automated system has demonstrated a significant decrease in the quantity of these defects when manufacturing these geometries (Figure 5c). The improvement is attributed to the precise control of the electrode movement, with the automated system able to specify both location and travel speed with greater accuracy and consistency than an operator can achieve on a manual system. Additionally, since

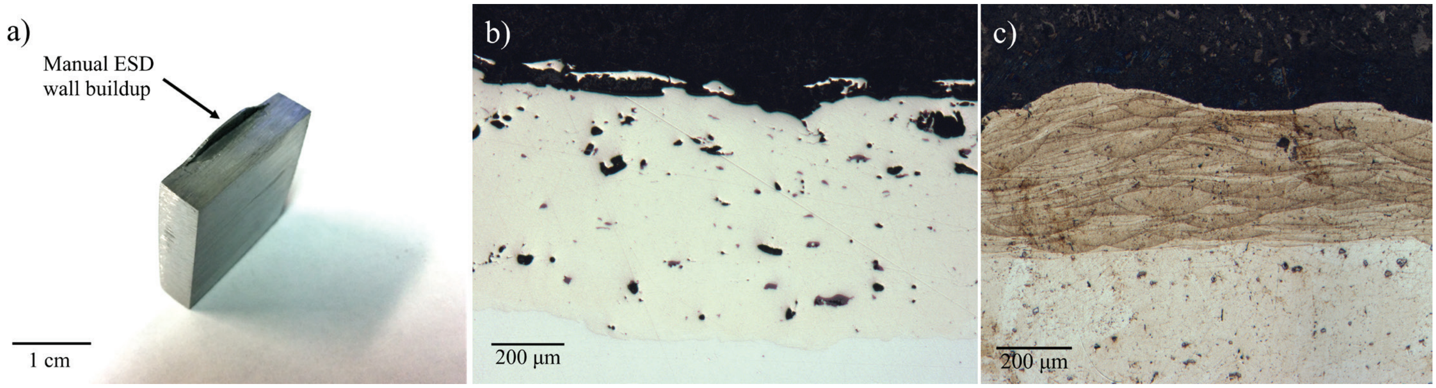

Fig. 5: Optical images of a) thin ridge buildup using manual ESD, b) cross-section of the ridge along the long axis, and c) etched cross-section of ridge along the long axis built with an automated ESD system.

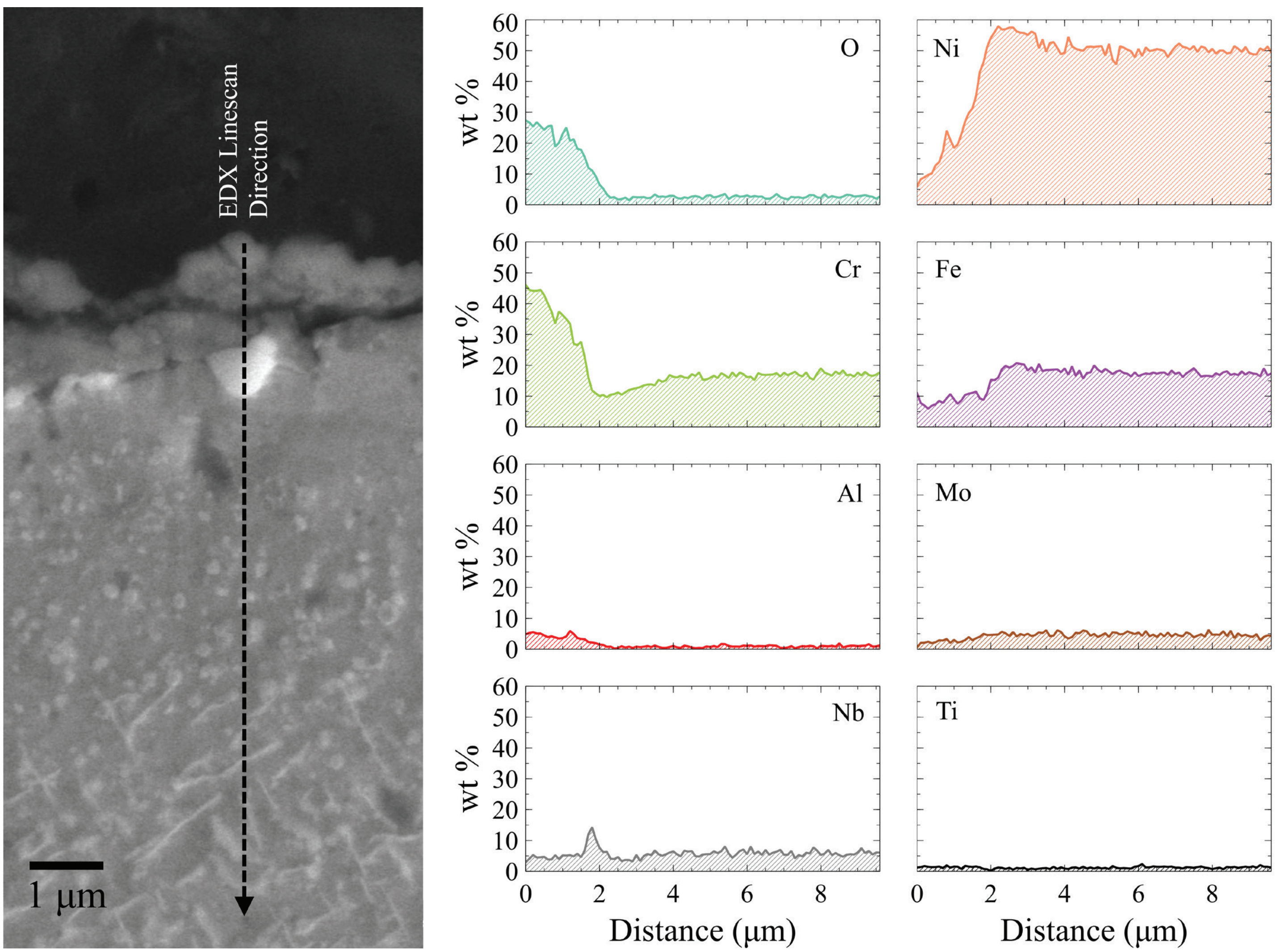

Fig. 6: Etched cross-section of oxide scale in ESD Inconel 718 after 24 h in air at 800 °C and EDX linescan results.

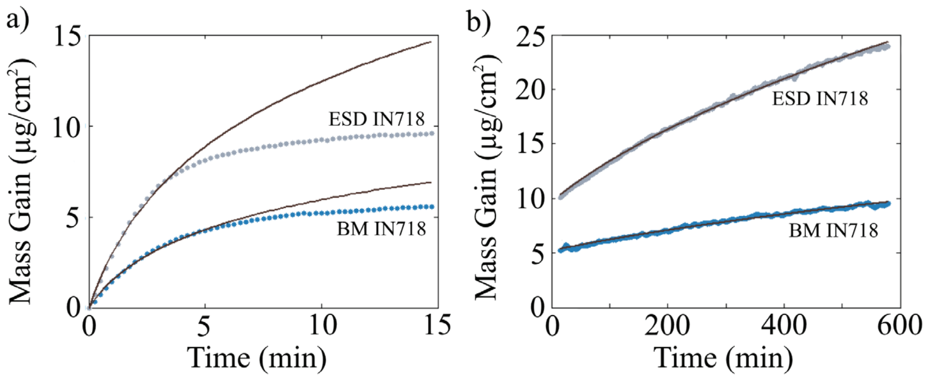

Fig. 7: Mass gain curves and model fits for ESD processed and base metal Inconel 718 oxide growth at 800°C during a) the initial growth phase and b) after formation of a passivating scale.

TABLE 2. FIT PARAMETERS FOR THE BEST FIT EQUATIONS IN FIGURE 7

Model	Material	$A\left(\frac{\mu g^2}{cm^2}\right)$	$B\left(\frac{1}{min}\right)$	R^2	Model applicability
Logarithmic	Base Metal	2.93	0.67	0.997	0 - 5.25 min
	ESD	6.92	0.53	0.997	0 - 3.75 min
Model	Material	$K_p\left(\frac{\mu g^2}{cm^4\,min}\right)$	$C\left(\frac{\mu g^2}{cm^4}\right)$	R^2	Model applicability
Parabolic	Base Metal	0.11	27.10	0.991	>15 min
	ESD	0.86	93.60	0.999	>15 min

these thin structures result in less effective heat transfer from the deposition surface, they benefit from lower voltage and capacitance parameters due to the lower heat input. This increases the build time and makes the use of an automated system more appealing.

3.3 Oxidation behaviour

The oxidation of ESD processed Inconel 718 at elevated temperatures in an air environment is also evaluated and compared to base metal Inconel 718. As expected, the formation of an oxide layer is observed (Figure 6). The high concentration of Cr suggests the scale consists primarily of a Cr-rich oxide [6], with the depletion of Cr in the substrate indicating that outward diffusion of Cr occurs when forming the oxide scale. Additionally, the formation of internal Nb-rich oxides at the interface between the Cr oxide scale and Inconel 718 are detected. Enrichment of the oxide scale with Al and the presence of other elements suggest that oxides beyond the primary Cr_2O_3 may form [7–9]. Although both the ESD Inconel 718 and base metal Inconel 718 show similar oxide composition, differences between the oxide thicknesses are observed. The oxide that forms on the ESD processed Inconel 718 is approximately twice as thick as the base metal Inconel 718.

Experimental mass gain measurements obtained by TGA of base metal and ESD Inconel 718 at 800°C are shown in Figure 7, with two periods showing distinctly different oxidation rate kinetics. As is typically observed in literature, Ni-superalloys similar to Inconel 718 rapidly react to form an oxide according to logarithmic kinetics (indicated by the black best-fit lines in Figure 7a), after which it transitions to the desired parabolic kinetics (Figure 7b) [10]. The initial rapid oxide formation is rarely studied in detail since it occurs rapidly, requires precise measurements, and is typically of little concern to the overall lifespan of the part. However, in a component exposed to an abrasive high-temperature environment, the ability to rapidly form an oxide scale is important.

Logarithmic oxidation kinetics are often used to describe initial oxide growth [16], which in this case has a thickness between 500 nm and 1 μm. The kinetics are observed in the form of:

$$m=A\ ln(1+Bt)$$

where m is the mass of the sample, t is the time, and A and B are constants. Although many theories have been proposed to describe logarithmic oxidation kinetics, none are fully accepted [17]. Parabolic growth kinetics are commonly used to describe the oxidation rate of high temperature materials that form passivating films [18]. Inconel 718 has been shown to form a chromium oxide film that slows oxidation of the underlying metal, with the oxidation rate inversely dependent on the thickness of the film. Oxidation kinetics in this regime are controlled by diffusion processes and can be described by:

$$m^2=k_p\ t+C$$

where m is the mass of the sample, t is the time, k_p is the diffusion rate constant, and C is an integration constant. In Inconel 718, the diffusion of Cr during high temperature oxidation is known to occur preferentially along grain boundaries [19]. Therefore, the finer grain size and solidification microstructure of ESD processed Inconel 718 – which forms cellular subgrain structures – should allow for a faster rate of passivating oxide film formation than the base metal.

Experimental fits for these models are listed in Table 2. The R^2 values are listed to indicate the ability of the model to explain the observed mass gain; the R^2 values greater than 0.99 indicate that the models provide an excellent description of oxide film growth upon initial oxide formation and over periods of up to approximately 10 hours. Additionally, the visual differences in oxide thickness are quantified; ESD Inconel 718 experiences a faster initial oxidation rate and forms a thicker oxide coating than the base metal Inconel 718, although both follow parabolic kinetics that indicate a passivating effect. However, the effect of a fine grain structure in the metal may only be limited to the short-term oxidation kinetics. Other literature results of Ni-superalloys with high chromium content show that the metal grain size does not influence the long-term oxidation behavior [20], which is instead influenced by the oxide grain size [21].

4.0 CONCLUSIONS

The development of an electrospark deposition (ESD) process for the repair of Ni-superalloys was presented, with a focus on Inconel 718. Two main topics are investigated: process parameter selection and an evaluation of oxidation behaviour. Depending on the target application, the findings presented here can help guide the use of ESD in repair and coating applications.

- Optimized process parameters were selected by studying the effect of voltage and capacitance. It is concluded that lower capacitance and voltage results in depositions with fewer defects, at the expense of the deposition rate. A porosity of less than 1% is achieved with the chosen parameters. Both peening and parameter selection influence the extent of surface roughness, with post process grinding or polishing required to achieve roughness below 5 µm.

- The use of automated ESD systems with accurate control over the electrode movement, travel speed and contact force result in depositions with fewer lack of fusion defects. This improves the deposition quality when fabricating sub-millimeter thin ridges, which are otherwise challenging in manual systems that rely on operator skill. Additionally, lower capacitance and voltage parameters can be used on automated systems to achieve higher quality depositions without having to consider the difficulties attributed to long deposition times for manually operated systems.

- Oxidation behaviour of ESD processed Inconel 718 is compared to the base metal, which shows that the ESD processed Inconel 718 more rapidly forms a chromium oxide scale. This is attributed to the fine solidification microstructure commonly found in ESD processed materials, which allows for the faster diffusion of chromium. Both the deposited and base metal Inconel 718 show logarithmic oxide growth kinetics during the initial stages, which then transition to parabolic kinetics that indicate the formation of a passivating film. W

▶ **Pablo D. Enrique [a], Zhen Jiao [b], Stephen Peterkin [b], Norman Y. Zhou [a],**
[a] University of Waterloo, [b] Huys Industries Ltd.,

Acknowledgment
This work was performed at the Centre for Advanced Materials Joining (CAMJ) at the University of Waterloo with funding support from the Natural Sciences and Engineering Research Council of Canada (NSERC), the Canada Research Chairs (CRC) Program, Huys Industries,and the CWB Welding Foundation.

References
[1] C.J. Chen, M.C. Wang, D.S. Wang, H.S. Liang, P. Feng, Characterisations of electrospark deposition Stellite 6 alloy coating on 316L sealed valve used in nuclear power plant, Mater. Sci. Technol. 26 (2010) 276–280 doi:10.1179/174328409X430447.
[2] W. Ruijun, W. Weiping, L. Yufen, T. Hehong, Repair heavy-duty generator rotor shaft by electro spark deposition process, Trans. JWRI. 39 (2010) 164–165. http://hdl.handle.net/11094/10 806.
[3] B.D. Sartwell, K.O. Legg, N. Price, D. Aylor, V. Champagne, M. Pepi, T. Pollard, Electrospark Deposition for Depot- and Field-Level Component Repair and Replacement of Hard Chromium Plating, 2008. http://www.dtic.mil/docs citations/ADA603502.
[4] V. Champagne, M. Pepi, B. Edwards, Electrospark Deposition for the Repair of Army Main Battle Tank Components, (2006).
[5] H.P. Bloch, F.K. Geitner, Machinery Component Maintenance and Repair, Elsevier, 2004.
[6] P.D. Enrique, Z. Jiao, N.Y. Zhou, Effect of Direct Aging on Heat-Affected Zone and Tensile Properties of Electrospark-Deposited Alloy 718, Metall. Mater. Trans. A. (2018). doi:10.1007/s11661-018-4997-1.
[7] P.D. Enrique, Z. Jiao, N.Y. Zhou, E. Toyserkani, Dendritic coarsening model for rapid solidification of Ni-superalloy via electrospark deposition, J. Mater. Process. Technol. 258 (2018) 138–143. doi:10.1016/j.jmatprotec.2018.03.023.
[8] P.D. Enrique, Z. Jiao, N.Y. Zhou, E. Toyserkani, Effect of microstructure on tensile properties of electrospark deposition repaired Ni-superalloy, Mater. Sci. Eng. A. 729 (2018) 268–275. doi:10.1016/j.msea.2018.05.049.
[9] X. Cao, B. Rivaux, M. Jahazi, J. Cuddy, A. Birur, Effect of pre- and post-weld heat treatment on metallurgical and tensile properties of Inconel 718 alloy butt joints welded using 4 kW Nd:YAG laser, J. Mater. Sci. 44 (2009) 4557–4571. doi:10.1007/s10853-009-3691-5.
[10] L.M. Felix, C.C.F. Kwan, N.Y. Zhou, The Effect of Pulse Energy on the Defects and Microstructure of Electro-Spark-Deposited Inconel 718, Metall. Mater. Trans. A. 50 (2019) 4223–4231. doi:10.1007/s11661-019-05332-8.
[11] G. a. Greene, C.C. Finfrock, Oxidation of Inconel 718 in Air at High Temperatures, Oxid. Met. 55 (2001) 505–521 doi:10.1023/A:1010359815550.
[12] Q. Jia, D. Gu, Selective laser melting additive manufactured Inconel 718 superalloy parts: High-temperature oxidation property and its mechanisms, Opt. Laser Technol. 62 (2014) 161–171. doi:10.1016/joptlastec.2014.03.008.
[13] C. Juillet, A. Oudriss, J. Balmain, X. Feaugas, F. Pedraza, Characterization and oxidation resistance of additive manufactured and forged IN718 Ni-based superalloys, Corros. Sci. 142 (2018) 266–276. doi:10.1016/j.corsci.2018.07.032.
[14] K.A. Al-hatab, M.A. Al-bukhaiti, U. Krupp, M. Kantehm, Cyclic Oxidation Behavior of IN 718 Superalloy in Air at High Temperatures, Oxid. Met. 75 (2011) 209–228. doi:10.1007/s11085-010-9230-6.
[15] A.A. Vicente, J.R.S. Moreno, J.A.S. TenÓRio, A.B. Botelho, A.T.F.A. Santos, C.R. Espinosa, Comparison of behaviour to oxidation at high temperature of two superalloys: Inconel 713c and IC-50, Oxid. Commun. 41 (2018) 195–204.
[16] H.H. Uhlig, Initial oxidation rate of metals and the logarithmic equation, Acta Metall. 4 (1956) 541–554. doi:10.1016/0001-6160(56)90051-7.
[17] M. Danielewski, Kinetics of Gaseous Corrosion Processes, Corros. Fundam. Testing, Prot. 13 (2018) 97–105. doi:10.31399/asm.hb.v13a.a0003589.
[18] D.J. Young, High Temperature Oxidation and Corrosion of Metals, Second Edi, Elsevier, 2008. http://www.sciencedirect.com/science/article/pii/B9780081001011050019.
[19] L. Li, X. Gong, X. Ye, J. Teng, Y. Nie, Y. Li, Q. Lei, Influence of building direction on the oxidation behavior of Inconel 718 alloy fabricated by additive manufacture of electron beam melting, Materials (Basel). 11 (2018). doi:10.3390/ma11122549.
[20] X. Wang, J.A. Szpunar, Effects of grain sizes on the oxidation behavior of Ni-based alloy 230 and N, J. Alloys Compd. 752 (2018) 40–52. doi:10.1016/j.jallcom.2018.04.173.
[21] L. Bataillou, C. Desgranges, L. Martinelli, D. Monceau, Modelling of the effect of grain boundary diffusion on the oxidation of Ni-Cr alloys at high temperature, Corros. Sci. 136 (2018) 148–160. doi:10.1016/j.corsci.2018.03.001.